



Research articles

Large magnetostriction in chemically fabricated CoFe_2O_4 nanoparticles and its temperature dependence

U. Salazar-Kuri ^{a,*}, J.O. Estevez ^b, N.R. Silva-González ^a, U. Pal ^a

^a Instituto de Física, Benemérita Universidad Autónoma de Puebla, Apdo. Postal J-48, Puebla, Pue. 72570, Mexico

^b Departamento de Materia Condensada/Instituto de Física UNAM, Circuito de la Investigación Científica Ciudad Universitaria, C.P. 04510, Mexico



ARTICLE INFO

Article history:

Received 17 November 2017

Received in revised form 28 March 2018

Accepted 31 March 2018

Available online 31 March 2018

Keywords:

Ferromagnetic

Spinel structure

Superparamagnetism

ABSTRACT

Cobalt ferrite nanoparticles were synthesized by co-precipitation technique from nitrate precursors. X-ray diffraction confirms the formation of the spinel ferrite. SEM and HRTEM micrographs corroborate the formation of agglomerated nanoparticles of 8–35 nm size range with 21.7 nm average size. The broad size distribution and considerable agglomeration of the particles hamper the superparamagnetic state of the sample, provoking a weak coercivity at room temperature. In contrast to several other magnetic nanostructures, the ZFC-FC curves of cobalt-ferrite nanoparticles revealed an unusually large magnetostriction, evidenced by larger values of magnetization in their ZFC curves than the FC curves in the measured temperature range 20–375 K. The behavior could be reversed on applying high magnetic fields. However, the maximum of ZFC curve reduces on increasing the applied magnetic field.

© 2018 Elsevier B.V. All rights reserved.

1. Introduction

Cobalt ferrite (CoFe_2O_4) belongs to the inverse spinel ferrites where Co^{2+} ions occupy the octahedral sites of lattice structure and half of the Fe^{3+} cations occupy octahedral sites and the other half stay at the tetrahedral sites of a fcc lattice formed by the oxygen ions [1]. It is a well-known hard magnetic material with moderate magnetization, high coercivity, high Curie temperature and large magnetostrictive coefficient [2,3]. Beside these characteristics, high physical and chemical stability of cobalt ferrite make it technologically attractive for audio and videotape recording and other high frequency devices [4]. From the point of view of biomedicine, magnetic nanoparticles have been studied for applications in sensors, resonance imaging, magnetically guided drug delivery, and magnetic hyperthermia [5,6]. Depending on the desired application, their magnetic properties can be tailored by varying the particle size and morphology, or by doping [7,8].

On the other hand, several magnetic systems undergo irreversible order-disorder transitions under magnetic field, exhibiting difference between their field-cooled (FC) and zero-field-cooled (ZFC) susceptibilities. Polycrystalline magnetic materials contain microscopic magnetic domains separated by domain walls, frequently inducing magnetic anisotropy in low dimensional magnetic structures such as their thin films and nanoparticles. The anisotropic orientation of magnetic dipoles is necessary to

obtain a stable minimum energy in the system. Domain walls, the transition boundaries between the regions of nearly uniform magnetization are classified in two categories: Bloch walls and Néel walls. In the former, the magnetic dipoles rotate in such a way that the component of the magnetization perpendicular to the plane of the wall remains constant. In the later, the magnetic dipoles rotate in the plane [9]. For nanoparticles, there is a critical radius below which the formation of domain walls is not favored and each nanoparticle stay in single domain regime, i.e., when the particle size is small enough, the system becomes an assembly of uncoupled single-domain particles. As the thermal energy dominates, the magnetization process occurs only by magnetic dipole rotation. This behavior is known as superparamagnetism [10]. This model is known as the macrospin model, which is the result of the effective low-energy theory where the microscopic spins are tightly aligned due to the ferromagnetic exchange and is valid just for weak anisotropy. In the case of strong anisotropy, magnetization reversal takes place by nucleation and domain wall propagation [11]. Due to the anisotropy, only two magnetic orientations are possible, which are separated by an energy barrier. When thermal energy (T_E) is less than the energy barrier ($E_a = K_{\text{eff}}V$), spin blocking occurs, and there is no inversion of the spins. Furthermore, E_a increases as nanoparticles size increases due to its proportionality with volume (V). Superparamagnetism is caused by the transition of the spin blocking state to superparamagnetic state and therefore, highly dependent on the size distribution of the particles. That is the reason we encounter a broad range dispersion in the reported values of blocking temperature (T_B) of nanoparticles

* Corresponding author.

E-mail address: usalazar@ifuap.buap.mx (U. Salazar-Kuri).

of a particular material, and most of the magnetic nanoparticles cannot be in superparamagnetic regime above certain size [12].

In general, for superparamagnetic particles, below blocking temperature T_B , magnetic susceptibility during ZFC is low as the particles are not in thermal equilibrium and the magnetization is due to the change in orientation of the magnetic dipoles along the axes of easier magnetization. As the temperature is increased, the smaller particles become superparamagnetic, and they align in the direction of the applied field, increasing the net magnetization of the sample. On the other hand, in magnetic susceptibility during FC, the blocking state is frozen, orienting along the easy axis, and as consequence, magnetization is higher than in ZFC. When ZFC susceptibilities are almost the same or slightly larger than those of FC in some temperature range, it is attributed to the strong interactions or large magnetostriction [13,14].

In this paper we report an unusual behavior in the ZFC-FC curves of CoFe_2O_4 nanoparticles, where the magnetic susceptibility values of ZFC curves are larger than those of FC in the whole range of measured temperatures under weak applied magnetic field. The behavior reverses for the applied magnetic field above a certain value.

2. Materials and methods

2.1. Synthesis of CoFe_2O_4 nanoparticles

CoFe_2O_4 nanoparticles were prepared by co-precipitation following the procedure reported by Duong et al. [15]. Stoichiometric

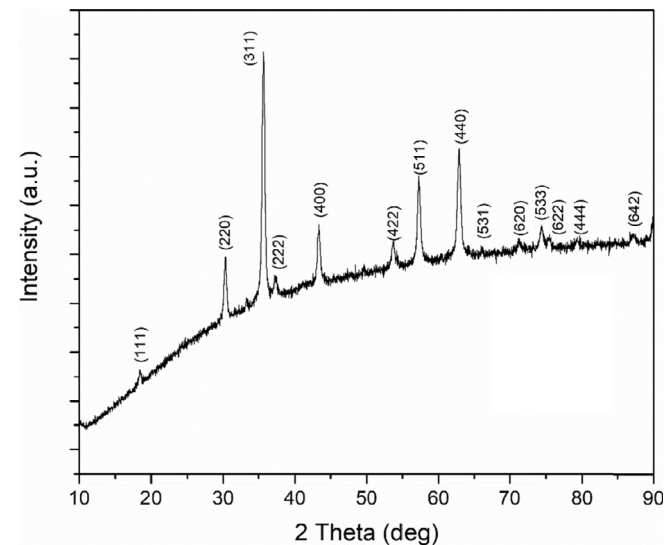


Fig. 1. XRD pattern of the annealed (500 °C 1 h) CoFe_2O_4 powders prepared by co-precipitation route. Diffraction peaks were indexed considering PDF file 22–1086.

amounts of cobalt nitrate hexahydrate $\text{Co}(\text{NO}_3)_2 \cdot 6\text{H}_2\text{O}$ and iron nitrate nonahydrate $\text{Fe}(\text{NO}_3)_3 \cdot 9\text{H}_2\text{O}$ were weighted and dissolved in deionized water. The mixture was heated to 70 °C and then a sodium hydroxide solution (NaOH 2.05 M) was added to it slowly under continuous mechanical stirring at 1000 rpm. The mixture was left in an isotherm (70 °C) for one hour. After cooling to room temperature, the precipitate was decanted and washed with deionized water until the pH reached to 7. Finally, the sample was dried at 80 °C for several hours and afterwards calcined in air at 500 °C for 1 h, to obtain it in powder form.

2.2. Characterization of the ceramic

The phase identification of the sample was performed by powder X-ray diffraction (XRD) using a PANalytical X-ray Empyrean diffractometer with Cu-K_α radiation ($\lambda = 1.5406 \text{ \AA}$) at 45 kV and 40 mA. Particle size and morphology were analyzed using a Jeol JSM-7800F field emission scanning electron microscope and a Jeol JEM-2010F high resolution transmission electron microscope (HRTEM). Magnetic measurements of the ceramic were performed in a Dynacool-9 physical properties measurement system (PPMS) of Quantum Design, with VSM (vibrating sample magnetometer) option. For magnetic characterization, the magnetization vs. magnetic field hysteresis curves of the powder sample were recorded between 1.8 and 378 K, under applied magnetic field up to 3.0 T. The field cooling (FC) and zero field cooling (ZFC) curves of the sample were recorded under 0.01, 0.05, 0.1, 0.15, 0.5 and 1.0 T applied field, in the temperature range 20–375 K.

3. Results and discussion

Fig. 1 shows the XRD pattern of the powder sample synthesized by co-precipitation technique and annealed at 500 °C. Revealed diffraction peaks are consistent with the reported data for spinel ferrite CoFe_2O_4 (PDF cards # 22–1086). Absence of additional peaks associated to any other phases or impurities indicates the phase purity of the sample. The positive slope in the background is product of the X-ray fluorescence of the sample when Cu radiation impinge Co and Fe.

Typical morphology of CoFe_2O_4 powder sample after annealing at 500 °C is presented in **Fig. 2**. As can be seen from the micrographs, the sample consists of agglomerated and dispersed semi-spherical particles of 8–35 nm sizes with average size (c.a.) 22 nm. As mention above, superparamagnetic transition has a high dependence on particle size. So, a broad size distribution of the nanoparticles implies a broad range of T_B values. As some of our nanoparticles are within the reported size range (<12 nm), a multidomain to single domain transition for the CoFe_2O_4 nanoparticles is expected at temperatures slightly above the room temperature [16,17].

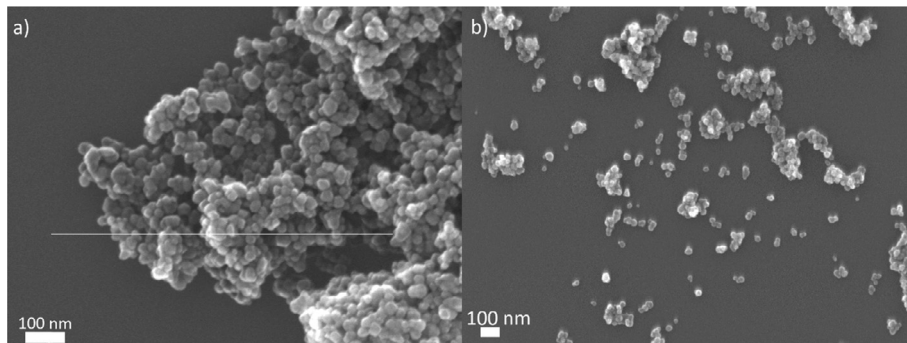


Fig. 2. Typical SEM micrographs of a) agglomerated and b) dispersed CoFe_2O_4 nanoparticles.

The morphology and crystallinity of the synthesized cobalt ferrite were studied further through TEM analysis. Typical TEM and HRTEM images of the sample are presented in Fig. 3. The average particle size estimated from TEM images was 21.7 nm, very close to the average size value obtained from SEM analysis. A typical HRTEM micrograph of the sample is shown in Fig. 3b. Crystallographic characteristics of the synthesized nanoparticles were identified by measuring the interplanar spacing, d , using the software digital micrograph 3.7.0. Fig. 3b presents CoFe_2O_4 particles with orientations along (4 0 0), (2 2 0) and (1 1 1) crystalline planes.

Fig. 4 depicts the magnetization (M) vs applied field (H) curves of the sample up to 3 T at different temperatures in an interval of 1.8–378 K. The saturation magnetization (M_s) is around 60 (emu/g) for low temperatures and 52 (emu/g) for room temperature and above. The coercive field (H_c) is strongly influence by temperature change (Fig. 4 inset). The coercivity decrease with temperature is due the increase of thermal energy that favors the orientation of magnetic dipoles along the applied field [18]. Above room temperature, the sample still shows paramagnetism with weak coercive field, but not superparamagnetism, probably due to the broad dis-

persion of particle size and agglomeration. Room temperature value are in good agreement with other reports [7,19].

The ZFC and FC magnetization curves of the cobalt ferrite sample measured in between 20 and 350 K under 0.01, 0.05, 0.1, 0.15, 0.5 and 1.0 T applied magnetic field are presented in Fig. 5. In general, for higher applied fields, all the FC magnetization curves remains almost independent over the whole range of temperatures with a slightly negative slope at high temperatures due to the spin orientation along the applied field. However below 100 K, the FC magnetization tends to saturate. On the other hand, a very unusual behavior was observed on decreasing the applied magnetic field to 0.05 T or lower. The ZFC curves of the sample revealed higher magnetization than its FC curves. We observed such magnetic behavior previously [20] in the solid solution $\text{Co}_{1-x}\text{Ni}_x\text{Fe}_2\text{O}_4$ which is less significant when Ni content is increased and finally curves start to flipped out (i.e. the FC curve is over the ZFC curve) at $x = 0.8$. Other workers have also observed such behavior (higher magnetization during ZFC than during FC) in $\text{La}_{0.275}\text{Pr}_{0.35}\text{Ca}_{0.375}\text{MnO}_3$ [13], $(\text{LaNd})\text{CaMnO}$ manganites [21], silica-coated akaganeite nanorods [22], S-doped graphene [23], Sm-doped TiO_2 nanorods [24] in a

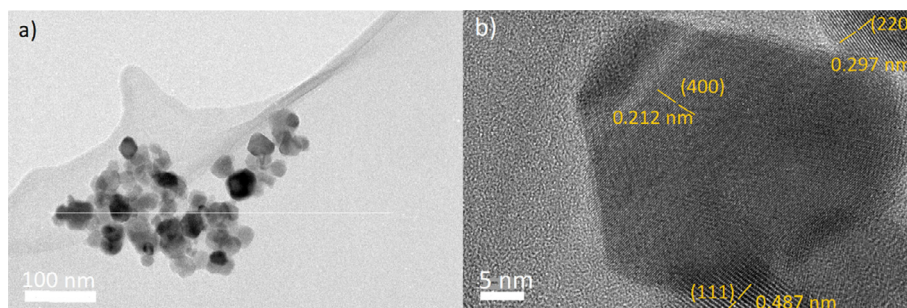


Fig. 3. Typical a) TEM and b) HRTEM micrographs for CoFe_2O_4 nanoparticles.

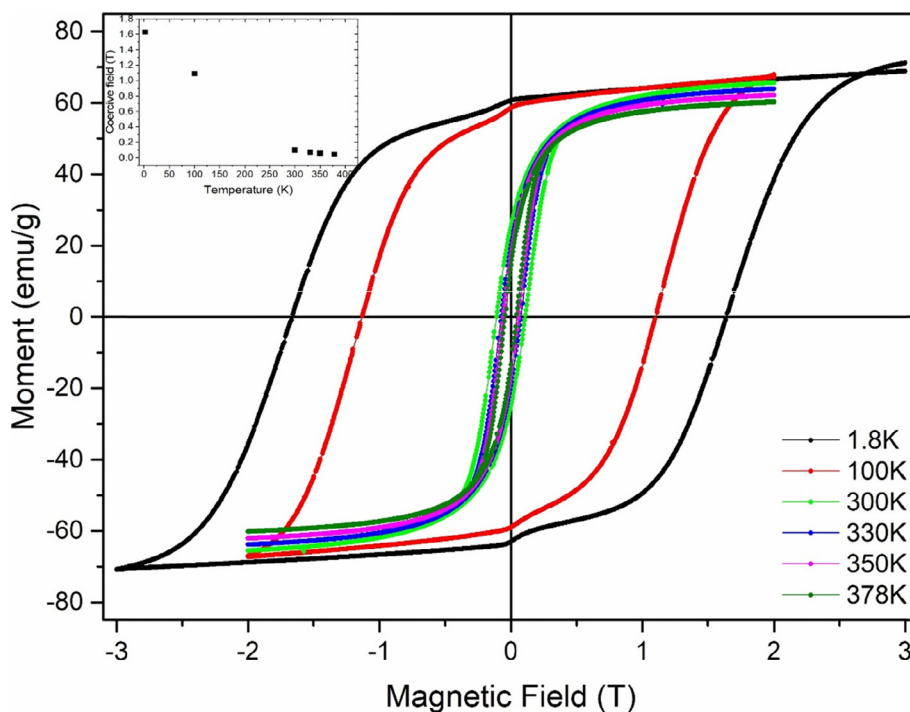


Fig. 4. Magnetization hysteresis loop for CoFe_2O_4 at different temperatures up to a maximum applied field of 2 T (3 T for 1.8 K). Inset shows the variation of coercivity (H_c) as function of temperature.

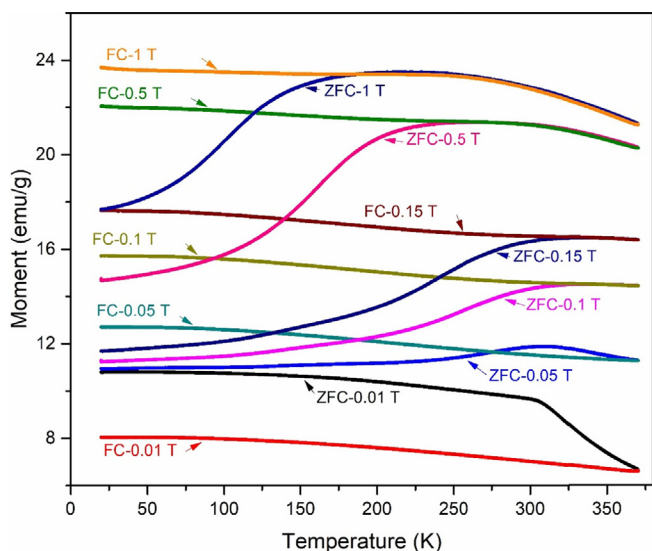


Fig. 5. ZFC and FC plots for the CoFe_2O_4 at 0.01, 0.05, 0.1, 0.15, 0.5 and 1 T applied magnetic field.

certain range of temperature where the ZFC curves have higher magnetization than FC curves, but not for cobalt ferrite. As mentioned above, this behavior has been associated to the high magnetostriction [13] or strong interactions between the particles [25]. In a magnetostrictive material when a magnetic field is applied on the ferromagnetic crystal, the domain walls shift and domains move, causing a change in the dimensions of the material due to the magnetocrystalline anisotropy. In other words, the material tends to arrange its structure in a way that the easy axis is aligned along the applied field direction. Different from the mentioned reports, in this work the large magnetostriction is present in the whole range of measured temperatures. When the applied field is decreased to 0.05 T, at lower temperatures, the ZFC and FC curves get merged. Moreover, for 0.01 T applied field, the curves flip-out (ZFC magnetization higher than FC magnetization) for the whole range of measured temperature.

As can be seen from Fig. 5, for higher applied fields (0.15, 0.5 and 1.0 T), the divergence between the FC–ZFC curves increases with applied field, especially at lower temperatures. On the other hand, the maximum position of ZFC increases on lowering the applied field up to 0.1 T (Table 1).

As mentioned above, the dispersion in particle size and agglomeration of some particles (as observed by FESEM and TEM micrographs), which increase the interaction between the particles, provoke the weak coercive field without achieving superparamagnetic state. Due to the same reasons, the maximum of ZFC are not sharp or well defined and cannot be designated as blocking temperature

Table 1 shows how the maximum of ZFC curves changes as function of applied field. At higher applied magnetic fields the energy required for spin inversion is lower. However, at lower

Table 1
Maximum of ZFC curve as function of applied magnetic field.

Applied field [T]	Maximum of ZFC [K]
0.01	303
0.05	305
0.10	315
0.15	316
0.50	276
1.0	235

applied magnetic fields, the effect of magnetostriction is prominent, which not only causes a reversal of FZC–FC magnetization, but also reduces the ZFC maximum.

Several authors have synthesized and characterized CoFe_2O_4 using ZFC–FC magnetization curves [6,26–29]. Most of them obtained different magnetic features depending on the synthesis method, the morphology and particle size. The results not only emphasize the importance of continuing exploration of magnetic behaviors of multiferroic nanoparticles such as CoFe_2O_4 , but also the choice of their synthesis method for desired applications.

4. Conclusion

CoFe_2O_4 nanoparticles were synthesized by co-precipitation technique. The ceramic showed an unusually large magnetostriction in the whole range of measured temperatures (20–375 K) that can be overcome by increasing the applied magnetic field. The large magnetostriction in a broad range of temperatures can be very useful when a mechanical coupling is required in multiferroic composite systems.

Acknowledgements

The work was financially supported by the SEP (Grant # SEP-DSA/103.5/16/10420), CONACYT (Grants # INFR-2011-1-1163153, and INFR-2014-02-23053), Mexico. The authors acknowledge Dr. Ma. Eunice De Anda Reyes for her technical support in performing magnetic measurements of the nanostructures.

Appendix A. Supplementary data

Supplementary data associated with this article can be found, in the online version, at <https://doi.org/10.1016/j.jmmm.2018.03.074>.

References

- [1] A. Goldman, *Modern Ferrite Technology*, second ed., Springer, Pittsburgh, PA, USA, 2006.
- [2] P.C. Rajath, R.S. Manna, D. Banerjee, M.R. Varma, K.G. Suresh, A.K. Nigam, *J. Alloys Compd.* 453 (2008) 298.
- [3] J. Wang, T. Deng, Y. Dai, *J. Alloys Compd.* 419 (2006) 155.
- [4] X. Meng, H. Li, J. Chen, L. Mei, K. Wang, X. Li, *J. Magnet. Mater.* 321 (2009) 1155.
- [5] M. Arruebo, R.F. Pacheco, M.R. Ibarra, J. Santamaria, *Nano Today* 2 (2007) 22.
- [6] T.E. Torres, A.G. Roca, M.P. Morales, A. Ibarra, C. Marquina, M.R. Ibarra, G.F. Goya, *J. Phys. Conf. Series* 200 (2010) 072101.
- [7] K. Maaz, W. Khalid, A. Mumtaz, S.K. Hasanain, J. Liu, J.L. Duan, *Physica E* 41 (2009) 593.
- [8] Y.I. Kim, D. Kim, C.S. Lee, *Physica B* 337 (2003) 42.
- [9] E.J. Torok, A.L. Olson, H.N. Oredson, *J. Appl. Phys.* 36–4 (1965) 1394.
- [10] B. Cinzia, P. Tiberto, *Magnetic hysteresis in nanostructured materials*, in: G. Bertotti, I.D. Mayergoyz (Eds.), *The Science of Hysteresis*, Elsevier, 2005, pp. 191–249, Chap. 2.
- [11] M. Sayad, D. Gütersloh, M. Potthoff, *Eur. Phys. J. B* 85 (125) (2012) 1.
- [12] F.A. Cardona, E.S. Urquiza, U. Pal, M.E.M. Álvarez, C.T. Duarte, G.N. Cherr, P. de la Presa, M.A.M. Rojas, *J. Magnet. Mater.* 441 (2017) 417.
- [13] B.C. Zhao, Y.Q. Ma, W.H. Song, Y.P. Sun, *Phys. Lett. A* 354 (2006) 472.
- [14] R.W. Chantrell, N.S. Walmsley, J. Gore, M. Maylin, *J. Appl. Phys.* 85 (1999) 4340.
- [15] G.V. Duong, R. Groessinger, R.S. Turtelli, *IEEE Trans. Magn.* 42–10 (2006) 3611.
- [16] A.G. Kolhatkar, A.C. Jamison, D. Litvinov, R.C. Willson, T.R. Lee, *Int. J. Mol. Sci.* 14 (2014) 15977–16009.
- [17] K.M. Krishnan, *IEEE Trans. Magn.* 46 (2010) 2523.
- [18] F.A. Cardona, K.R. Rojas, R. Costo, M.A.M. Rojas, A. Hernando, P. Presa, *J. Alloys Compd.* 663 (2016) 636.
- [19] C. Pereira, A.M. Pereir, C. Fernandes, M. Rocha, R. Mendes, M. Fernandez-garcia, A. Guedes, P.B. Tavares, J.M. Grenèche, J.P. Araujo, C. Freire, *Chem. Mater.* 24 (2012) 1496.
- [20] U. Salazar-Kuri, J.O. Estevez, R.R. Silva-González, U. Pal, M.E. Mendoza, *J. Magnet. Mater.* 442 (2017) 247.
- [21] L. Ghivelder, G.G. Eslava, R.S. Freitas, G. Leyva, F. Parisi, *J. Alloys Compd.* 680 (2016) 494.
- [22] M. Tadic, I. Milosevic, S. Kralj, M. Mbojji, L. Motte, *J. Phys. Chem. C* 119 (2015) 13868.

- [23] J. Zhu, H. Park, R. Podila, A. Wadehra, P. Ayala, L. Oliveira, J. He, A.A. Zakhidov, A. Howard, J. Wilkins, A.M. Rao, *J. Magnet. Magnet. Mater.* 401 (2016) 70.
- [24] L. Ting, X. Luo, S. Li, J. Yi, *J. Alloys Compd.* 687 (2016) 294.
- [25] R.W. Chantrell, N.S. Walmsley, J. Gore, M. Maylin, *J. Appl. Phys.* 85 (1999) 4340.
- [26] A. Chaudhuri, K. Mandal, *J. Magnet. Magnet. Mater.* 377 (2015) 441.
- [27] X.H. Li, C.L. Xu, L. Qiao, T. Wang, F.S. Li, *Nanoscale Res. Lett.* 5 (6) (2010) 1039.
- [28] K. Vasundhara, S.N. Achary, S.K. Deshpande, P.D. Babu, S.S. Meena, A.K. Tyagi, *J. Appl. Phys.* 113 (2013) 194101.
- [29] B.B. Stojic, V. Jokanovic, D. Milivojevic, Z. Jaglicic, D. Makovec, N. Jovic, M.M. Cincovic, *J. Nanomaterials* 2013 (2013) 741036.